An Efficient and Stable Solver for the Shallow Water Equations on Regular Latitude-Longitude Grids Using Spherical Fourier Transforms

Suzune Nomura[1(✉)] and Takeshi Enomoto[2]

[1] Graduate School of Science, Kyoto University, Kyoto 606-8502, Japan
nomura@dpac.dpri.kyoto-u.ac.jp
[2] Disaster Prevention Research Institute, Kyoto University, Uji 611-0011, Japan
enomoto.takeshi.3n@kyoto-u.ac.jp

Abstract. In this study, we apply a spatial differentiation method using the one-dimensional Fourier transform, along with an isotropic wavenumber truncation method based on the direct conversion between spherical Fourier and spherical harmonic coefficients, to the shallow water equations on a sphere. By utilizing the geometric properties of vectors at the poles and evaluating the limit as the colatitude approaches the poles, we successfully resolved the pole singularity problem. Consequently, this approach is applicable to regular latitude-longitude grids that include the poles.

Spatial differentiation is performed in an intermediate space between the physical and wavenumber spaces, without requiring a full transformation into the spherical Fourier space, whereas the wavenumber truncation is executed exclusively within the spherical Fourier space. The computational costs for these procedures are $O(N^2 \log N)$ and $O(N^3)$, respectively. These computations are highly parallelizable, enabling fast computation, and can be implemented without altering the basis functions of the Fourier transform. Furthermore, the intrinsic noise of the spherical Fourier transform is effectively removed by isotropic truncation, ensuring stable time integration.

Numerical experiments applying these methods to the shallow water equations demonstrate that the proposed approach yields smaller errors than conventional spherical harmonic transform methods in both linear and nonlinear problems. Moreover, parallelization using Fortran Coarrays achieved computational speeds comparable to those of the spherical harmonic transform. These findings indicate that our method, which does not require the spherical harmonic transform, is an efficient and highly accurate approach for solving time-dipendent partial differential equations on a sphere, including the polar regions.

Keywords: Pole singularity problem · Isotropic wavenumber truncation · Legendre transformation · Spectral methods on the sphere · Dynamical core · Parallel computing

© The Author(s), under exclusive license to Springer Nature Switzerland AG 2027
O. Gervasi et al. (Eds.): ICCSA 2026 Workshops, LNCS 16766, pp. 117–134, 2027.
https://doi.org/10.1007/978-3-032-30539-8_8

1 Introduction

In recent years, global atmospheric models worldwide have undergone significant advancements toward higher resolutions. For example, the dynamical core of the Global Spectral Model at the Japan Meteorological Agency was upgraded from TL349L40 to TL959L60 in 2007, and TQ959L128 is currently in operation as of March 2026 (where TL and TQ denote a linear grid and a quadratic grid, respectively). Furthermore, the spectral method is also employed in the models of the European Centre for Medium-Range Weather Forecasts. Because hydrostatic models primarily target large-scale phenomena such as jet streams, the spectral method, which can analytically calculate the derivatives of waves, is an extremely effective approach.

In conventional spectral methods on a sphere, the spherical harmonic transform has been predominantly used. However, its computational cost reaches $O(N^3)$, where N is the truncation wavenumber, making the enormous computational burden a bottleneck for achieving higher resolutions. To avoid this computational cost, an increasing number of global models are transitioning to local discretization schemes such as the finite volume or finite element method. Meanwhile, as an approach to improve computational efficiency while maintaining the high accuracy of wave resolution inherent in spectral methods, the spherical Fourier transform has been proposed [2–4,14,22]. These computational methods have a significant advantage in that their computational cost is $O(N^2 \log N)$ and they can utilize the widely used fast Fourier transform (FFT; [5,19]).

There have been several reports of constructing shallow water equation models using spherical Fourier transforms [17,24]. However, the method proposed by Spotz et al. [17] multiplied latitude-dependent metric coefficients (such as $1/\sin\theta$, where θ is the colatitude) on the physical grid. These coefficients appear in longitudinal differentiation on a sphere and cause singularities at the poles, making it impossible to place grid points exactly at the poles. Additionally, since Spotz et al. [17] relied on the spherical harmonic transform to achieve high accuracy equivalent to conventional spectral methods, the inherent computational bottleneck of the transform remained fundamentally unresolved. Unique wavenumber truncations based on the spherical Fourier transform were also proposed; however, these suffered from inferior computational accuracy and the inability to maintain isotropy on the sphere. In contrast, Yoshimura [24] introduced basis functions that include the latitudinally dependent coefficients and implemented them using the Galerkin method, successfully resolving the issue of being unable to place grid points at the poles. Nevertheless, the problem of isotropy in wavenumber truncation remains unresolved.

To address these remaining issues, in this paper, we derive a new formulation to accurately evaluate the gradient, vorticity, and divergence at the poles. Furthermore, for the isotropic wavenumber truncation method, we use a direct conversion from spherical Fourier coefficients to spherical harmonic coefficients, and apply a triangular truncation that mathematically guarantees isotropy on the sphere. Through these advancements, we propose a new highly accurate and

fast solver on a grid including the poles, constructed solely with Fourier transforms and coefficient conversions, thereby achieving computational efficiency.

The structure of this paper is as follows. Section 2 describes the formulation of spatial differentiation at the poles. Section 3 details the wavenumber truncation method that guarantees isotropy on the sphere. In Sect. 4, the new pseudospectral method based on the spherical Fourier transform, which combines the spatial differentiation method from Sect. 2 and the wavenumber truncation from Sect. 3, is applied to the shallow water equations. We then verify the accuracy of the proposed method through comparisons with the conventional spectral method using the spherical harmonic transform, as well as with a pseudospectral method that uses the spherical Fourier transform for spatial differentiation but the spherical harmonic transform for wavenumber truncation. Section 5 compares the execution times between the new spherical Fourier transform and the spherical harmonic transform, using a benchmark test that simplifies the computational process of the shallow water equations. Finally, Sect. 6 presents the conclusions.

2 Formulation on the Poles

For spatial differentiation away from the poles, similar to the method of Spotz et al. [17], one-dimensional Fourier transforms are applied along lines of latitude or longitude, differentiation operations are performed in wavenumber space, and the results are inversely transformed to obtain the derivative values in physical space. In this process, coefficients dependent on the radius of the latitude circle, which arise in calculations such as the longitudinal component of the gradient, are multiplied in physical space.

For differentiation in the longitudinal direction, periodicity is inherently guaranteed; therefore, the one-dimensional Fourier transform can be applied directly. For differentiation in the latitudinal direction, on the other hand, the latitudinal data array at a given longitude λ and the array at longitude $\lambda + \pi$ (shifted by π rad) are concatenated to form a periodic great circle passing through the North and South Poles. This makes it possible to apply the one-dimensional Fourier transform.

The method of Spotz et al. [17] targeted a regular latitude-longitude grid that does not include the poles, and prioritized ensuring a unified direction of differentiation along the great circle passing through the two poles. Consequently, when concatenating arrays across the poles, the signs for scalar fields were inverted, whereas those for vector fields were not. However, since our proposed method is designed to accommodate a grid that includes the poles, it is strictly required that the physical quantities be mathematically continuous at the poles to prevent the Gibbs phenomenon at these singular points. Due to the geometric properties of the spherical coordinate system, when a vector component (latitudinal or longitudinal wind velocity) crosses the pole to a longitude shifted by π rad, the orientation of the local coordinate axis is reversed, and the signs of concatenated vectors are also reversed. Therefore, to preserve physical

continuity at the poles, it is necessary to invert the signs of the concatenated arrays across the poles. This consideration is equivalent to reversing the signs of the derivatives in regions where the longitude is shifted by π, We employed this method.

2.1 The Longitudinal Component of the Gradient at the Poles

Denote the unit vector in Cartesian coordinates by ($\mathbf{i}$, $\mathbf{j}$, $\mathbf{k}$) and the unit vector in spherical coordinates by ($\mathbf{e}_r$, $\mathbf{e}_\theta$, $\mathbf{e}_\lambda$); this transformation can be expressed as follows:

$$\begin{pmatrix} \mathbf{e}_r \\ \mathbf{e}_\theta \\ \mathbf{e}_\lambda \end{pmatrix} = \mathbf{R} \begin{pmatrix} \mathbf{i} \\ \mathbf{j} \\ \mathbf{k} \end{pmatrix} = \mathbf{R}_y(\theta)\mathbf{R}_z(\lambda) \begin{pmatrix} \mathbf{i} \\ \mathbf{j} \\ \mathbf{k} \end{pmatrix} \tag{1}$$

where $\mathbf{R}_y(\theta)$ and $\mathbf{R}_z(\lambda)$ are the rotation matrices for the y-axis and z-axis, respectively. The transformation matrix $\mathbf{R}$ is given by

$$\mathbf{R} = \mathbf{R}_y(\theta)\mathbf{R}_z(\lambda) = \begin{pmatrix} \sin\theta & 0 & \cos\theta \\ \cos\theta & 0 & -\sin\theta \\ 0 & 1 & 0 \end{pmatrix} \begin{pmatrix} \cos\lambda & \sin\lambda & 0 \\ -\sin\lambda & \cos\lambda & 0 \\ 0 & 0 & 1 \end{pmatrix}$$

In particular, the transformation at the poles is given by

$$\begin{pmatrix} \mathbf{e}_r \\ \mathbf{e}_\theta \\ \mathbf{e}_\lambda \end{pmatrix} = \begin{cases} \mathbf{R}_y(0)\mathbf{R}_z(\lambda) \begin{pmatrix} \mathbf{i} \\ \mathbf{j} \\ \mathbf{k} \end{pmatrix} & \text{as } \theta \to 0 \text{ (north pole)} \\ \mathbf{R}_y(\pi)\mathbf{R}_z(\lambda) \begin{pmatrix} \mathbf{i} \\ \mathbf{j} \\ \mathbf{k} \end{pmatrix} & \text{as } \theta \to \pi \text{ (south pole)} \end{cases}$$

Therefore, at the North Pole, we have

$$\begin{aligned} \begin{pmatrix} \mathbf{e}_r \\ \mathbf{e}_\theta \\ \mathbf{e}_\lambda \end{pmatrix} &= \mathbf{R}_y(0)\mathbf{R}_z(\lambda) \begin{pmatrix} \mathbf{i} \\ \mathbf{j} \\ \mathbf{k} \end{pmatrix} \\ &= \begin{pmatrix} 0 & 0 & 1 \\ 1 & 0 & 0 \\ 0 & 1 & 0 \end{pmatrix} \begin{pmatrix} \cos\lambda & \sin\lambda & 0 \\ -\sin\lambda & \cos\lambda & 0 \\ 0 & 0 & 1 \end{pmatrix} \begin{pmatrix} \mathbf{i} \\ \mathbf{j} \\ \mathbf{k} \end{pmatrix} \\ &= \begin{pmatrix} 0 & 0 & 1 \\ \cos\lambda & \sin\lambda & 0 \\ -\sin\lambda & \cos\lambda & 0 \end{pmatrix} \begin{pmatrix} \mathbf{i} \\ \mathbf{j} \\ \mathbf{k} \end{pmatrix} \end{aligned}$$

Focusing on $\mathbf{e}_\theta$ and $\mathbf{e}_\lambda$, we obtain

$$\begin{pmatrix} \mathbf{e}_\theta \\ \mathbf{e}_\lambda \end{pmatrix} = \begin{pmatrix} \cos\lambda & \sin\lambda \\ -\sin\lambda & \cos\lambda \end{pmatrix} \begin{pmatrix} \mathbf{i} \\ \mathbf{j} \end{pmatrix}$$

Thus, $\mathbf{e}_\theta$ and $\mathbf{e}_\lambda$ at the North Pole are expressed as

$$\begin{aligned}\mathbf{e}_\theta(0,\,\lambda) &= \cos\lambda\mathbf{i} + \sin\lambda\mathbf{j}\\ \mathbf{e}_\lambda(0,\,\lambda) &= -\sin\lambda\mathbf{i} + \cos\lambda\mathbf{j} = \mathbf{e}_\theta\left(\lambda + \frac{\pi}{2}\right)\end{aligned} \tag{2}$$

Similarly, in South Pole are expressed as

$$\begin{aligned}\mathbf{e}_\theta(\pi,\,\lambda) &= -\cos\lambda\mathbf{i} - \sin\lambda\mathbf{j}\\ \mathbf{e}_\lambda(\pi,\,\lambda) &= -\sin\lambda\mathbf{i} + \cos\lambda\mathbf{j} = -\mathbf{e}_\theta\left(\lambda + \frac{\pi}{2}\right)\end{aligned} \tag{3}$$

Eqs. (2) and (3), considered on the unit circle, is applied to the gradient of an arbitrary scalar $f(\theta, \lambda)$.

$$\nabla f = \begin{pmatrix} \frac{\partial f}{\partial \theta} \\ \frac{1}{\sin\theta}\frac{\partial f}{\partial \lambda} \end{pmatrix} = \begin{pmatrix} \nabla f \cdot \mathbf{e}_\theta \\ \nabla f \cdot \mathbf{e}_\lambda \end{pmatrix} \tag{4}$$

Substituting Eqs. (2) and (3) into Eq. (4) obtains the longitude component of the gradient at the pole:

$$\begin{aligned}\lim_{\theta\to 0}\frac{1}{\sin\theta}\frac{\partial f}{\partial\lambda} &= \nabla f\cdot\mathbf{e}_\lambda\,(0,\,\lambda) = \nabla f\cdot\mathbf{e}_\theta\left(0,\,\lambda+\frac{\pi}{2}\right)\\ \lim_{\theta\to \pi}\frac{1}{\sin\theta}\frac{\partial f}{\partial\lambda} &= \nabla f\cdot\mathbf{e}_\lambda\,(\pi,\,\lambda) = -\nabla f\cdot\mathbf{e}_\theta\left(\pi,\,\lambda+\frac{\pi}{2}\right)\end{aligned} \tag{5}$$

This means that the longitudinal component of the gradient at the poles is a rotation of the latitudinal component.

2.2 The Vorticity and Divergence at the Poles

The vorticity ζ and divergence δ are fundamentally defined as the limits of circulation C and flux F per unit area ΔS, respectively. By substituting the differential forms of the operators in spherical coordinates and considering the surface element $\mathrm{d}S = \sin\theta\mathrm{d}\theta\mathrm{d}\lambda$ on the unit sphere, these definitions can be expressed as follows:

$$\begin{aligned}\zeta &= \lim_{\Delta S\to 0}\frac{\Delta C}{\Delta S} = \lim_{D\to 0}\frac{\int\int_D \frac{1}{\sin\theta}\left[\frac{\partial(\sin\theta u)}{\partial\theta} - \frac{\partial v}{\partial\lambda}\right]\sin\theta\mathrm{d}\theta\mathrm{d}\lambda}{\int\int_D \sin\theta\mathrm{d}\theta\mathrm{d}\lambda}\\ \delta &= \lim_{\Delta S\to 0}\frac{\Delta F}{\Delta S} = \lim_{D\to 0}\frac{\int\int_D \frac{1}{\sin\theta}\left[\frac{\partial(\sin\theta v)}{\partial\theta} + \frac{\partial u}{\partial\lambda}\right]\sin\theta\mathrm{d}\theta\mathrm{d}\lambda}{\int\int_D \sin\theta\mathrm{d}\theta\mathrm{d}\lambda}\end{aligned} \tag{6}$$

where $\mathbf{v}^{\mathrm{T}} = (u, v)$ is the velocity vector. The cancellation of $\sin\theta$ terms within this integral representation ensures that ζ and δ remain finite, providing a robust

mathematical basis for our treatment of the poles and justifying their global representation through the following limits:

$$\zeta = \begin{cases} \lim\limits_{\theta\to 0} \dfrac{\int_0^{2\pi}\int_0^{\theta} \frac{1}{\sin\theta'}\left[\frac{\partial\left(\sin\theta' u\right)}{\partial\theta'} - \frac{\partial v}{\partial\lambda}\right]\sin\theta' \mathrm{d}\theta'\mathrm{d}\lambda}{\int_0^{2\pi}\int_0^{\theta}\sin\theta'\mathrm{d}\theta'\mathrm{d}\lambda} & \text{for } \theta = 0 \\ \dfrac{1}{\sin\theta}\left[\dfrac{\partial\left(\sin\theta u\right)}{\partial\theta} - \dfrac{\partial v}{\partial\lambda}\right] & \text{for } 0 < \theta < \pi \\ \lim\limits_{\theta\to \pi} \dfrac{\int_0^{2\pi}\int_0^{\theta} \frac{1}{\sin\theta'}\left[\frac{\partial\left(\sin\theta' u\right)}{\partial\theta'} - \frac{\partial v}{\partial\lambda}\right]\sin\theta' \mathrm{d}\theta'\mathrm{d}\lambda}{\int_0^{2\pi}\int_0^{\theta}\sin\theta'\mathrm{d}\theta'\mathrm{d}\lambda} & \text{for } \theta = \pi \end{cases} \tag{7}$$

$$\delta = \begin{cases} \lim\limits_{\theta\to 0} \dfrac{\int_0^{2\pi}\int_0^{\theta} \frac{1}{\sin\theta}\left[\frac{\partial(\sin\theta v)}{\partial\theta} + \frac{\partial u}{\partial\lambda}\right]\sin\theta \mathrm{d}\theta\mathrm{d}\lambda}{\int_0^{2\pi}\int_0^{\theta}\sin\theta\mathrm{d}\theta\mathrm{d}\lambda} & \text{for } \theta = 0 \\ \dfrac{1}{\sin\theta}\left[\dfrac{\partial\left(\sin\theta v\right)}{\partial\theta} + \dfrac{\partial u}{\partial\lambda}\right] & \text{for } 0 < \theta < \pi \\ \lim\limits_{\theta\to \pi} \dfrac{\int_0^{2\pi}\int_0^{\theta} \frac{1}{\sin\theta'}\left[\frac{\partial\left(\sin\theta' v\right)}{\partial\theta'} + \frac{\partial u}{\partial\lambda}\right]\sin\theta' \mathrm{d}\theta'\mathrm{d}\lambda}{\int_0^{2\pi}\int_0^{\theta}\sin\theta'\mathrm{d}\theta'\mathrm{d}\lambda} & \text{for } \theta = \pi \end{cases} \tag{8}$$

Applying L'Hôpital's rule to evaluate this limit yields for the vorticity and divergence at the poles, respectively:

$$\zeta = \begin{cases} \dfrac{1}{\pi}\displaystyle\int_0^{2\pi} \left.\frac{\partial u}{\partial\theta}\right|_{\theta=0} \mathrm{d}\lambda & \text{for } \theta = 0 \\ \dfrac{1}{\pi}\displaystyle\int_0^{2\pi} \left.\frac{\partial u}{\partial\theta}\right|_{\theta=\pi} \mathrm{d}\lambda & \text{for } \theta = \pi \end{cases} \tag{9}$$

$$\delta = \begin{cases} \dfrac{1}{\pi}\displaystyle\int_0^{2\pi} \left.\frac{\partial v}{\partial\theta}\right|_{\theta=0} \mathrm{d}\lambda & \text{for } \theta = 0 \\ \dfrac{1}{\pi}\displaystyle\int_0^{2\pi} \left.\frac{\partial v}{\partial\theta}\right|_{\theta=\pi} \mathrm{d}\lambda & \text{for } \theta = \pi \end{cases} \tag{10}$$

This result is consistent with the fact that, at the poles, the longitudinal component u represents rotation and the latitudinal component v represents divergence, meaning that vorticity and divergence can be expressed solely in terms of these respective components.

2.3 The Laplacians at the Poles

The scalar Laplacian and the vector Laplacian are expressed as follows, respectively [20]:

$$\begin{aligned} \Delta_s f &= \nabla \cdot (\nabla f) \\ \Delta_v \mathbf{f} &= \nabla(\nabla \cdot \mathbf{f}) + \mathbf{k} \times \nabla \left(\mathbf{k} \cdot \nabla \times \mathbf{f}\right) \end{aligned} \tag{11}$$

Here, f and $\mathbf{f}$ are represent an arbitrary scalar and vector, respectively, where $\mathbf{k}$ is the unit vector in the z-axis (i.e., $\mathbf{k}^{\mathrm{T}} = (0, 0, 1)$). While the scalar and vector Laplacians typically involve singularities at the poles, it is possible to obtain finite values by employing formulations for the gradient, vorticity, and divergence that do not diverge (see Sect. 2.1 and 2.2).

3 Formulation of Isotropic Wavenumber Truncation

In previous studies, when solving time-dependent partial differential equations on the sphere using the spherical Fourier transform, pseudo-spectral methods (e.g., [3,17]) and Galerkin spectral methods (e.g., [24]) have been employed. Both approaches require wavenumber truncation to remove high-frequency components generated by nonlinear terms. Wavenumber truncation based on the 3/2 rule in Fourier space for de-aliasing exhibit the following characteristics:

- It cannot entirely eliminate the inherent noise errors near the poles caused by the use of the spherical Fourier transform.
- While spherical harmonics guarantee isotropy on a sphere, Fourier series only guarantee isotropy on a torus.

Due to these characteristics, the importance of applying a filter based on the spherical harmonic transform has been pointed out when using the spherical Fourier transform for spatial differentiation.

3.1 Isotropic Wavenumber Truncation of Scalar Fields

The associated Legendre functions, which constitute spherical harmonics, can be Fourier-transformed [11,12,16]. Consequently, spherical harmonic coefficients can be derived directly from Fourier coefficients [9,10].

Let $\mathrm{ar}_{n,m}$ and $\mathrm{ai}_{n,m}$ be the spherical harmonic coefficients, and $A_{k,m}$ and $B_{k,m}$ be the spherical Fourier coefficients defined by Yee [22]. The transformation between these coefficients is expressed as:

$$A_{k,m} = \sum_{\substack{n=\max(m,k) \\ n-k \in \mathrm{even}}}^{N} p_{n,m,k} \mathrm{ar}_{n,m}, \qquad B_{k,m} = \sum_{\substack{n=\max(m,k) \\ n-k \in \mathrm{even}}}^{N} p_{n,m,k} \mathrm{ai}_{n,m} \tag{12}$$

and the corresponding inverse transform:

$$\mathrm{ar}_{n,m} = \sum_{k=0}^{N} q_{n,m,k} A_{k,m}, \qquad \mathrm{ai}_{n,m} = \sum_{k=0}^{N} q_{n,m,k} B_{k,m} \tag{13}$$

where, $p_{n,m,k}$ and $q_{n,m,k}$ are a function that does not depend on colatitude θ or longitude λ, a precomputable array.

For a triangular truncation with a wavenumber $N_{\mathrm{TR}}(\leq N)$, it suffices to evaluate the transformation up to $n = N_{\mathrm{TR}}$. Therefore, the wavenumber truncation for a given scalar function f is performed according to the following procedure:

1. Apply the spherical Fourier transform to the scalar function $f(\theta, \lambda)$. For a given zonal wavenumber m $(0 \leq m \leq N_{\mathrm{TR}})$, we obtain the coefficients $A_{k,m}$ and $B_{k,m}$ $(0 \leq k \leq N_{\mathrm{TR}})$, which satisfy:

$$\tilde{f}(\theta, \lambda) = \sum_{m=0}^{N_{\mathrm{TR}}} \sum_{k=0}^{N_{\mathrm{TR}}} h_m(k\theta) \left(A_{k,m} \cos m\lambda + B_{k,m} \sin m\lambda\right)$$

   where N_{TR} is the maximum wavenumber and

$$h_m(\psi) \equiv \begin{cases} \cos\psi & \text{if } m \text{ is even} \\ \sin\psi & \text{if } m \text{ is odd} \end{cases}$$

   is a function defined conditionally based on the parity of m.
2. Transform $A_{k,m}$ and $B_{k,m}$ into $\mathrm{ar}_{n,m}$ and $\mathrm{ai}_{n,m}$.
3. Reconstruct $\tilde{A}_{k,m}$ and $\tilde{B}_{k,m}$ from the truncated spherical harmonic coefficients obtained in Step 2.
4. Perform the inverse spherical Fourier transform using $\tilde{A}_{k,m}$ and $\tilde{B}_{k,m}$ obtain the filtered physical data.

The coefficients $\tilde{A}_{k,m}$ and $\tilde{B}_{k,m}$ obtained in Step 3 are generally distinct from the original $A_{k,m}$ and $B_{k,m}$ in Step 2. This is because an associated Legendre function is represented by a finite cosine series, meaning that a single spherical harmonic component is projected onto multiple wavenumbers within the spherical Fourier space. By performing the transformations in Step 2 and Step 3, the resulting coefficients $\tilde{A}_{k,m}$ and $\tilde{B}_{k,m}$ are no longer affected by the projection of spectra that reside in the truncated region of the spherical harmonic space.

3.2 Isotropic Wavenumber Truncation of Vector Fields

By leveraging the isotropic wavenumber truncation for scalar fields described in Sect. 3.1, the truncation of vector fields can be achieved through Helmholtz decomposition. This process is performed according to the following procedure:

1. Compute the vorticity and divergence from the wind velocity vector.
2. Apply the spherical Fourier transform to the vorticity and divergence to obtain their respective spherical Fourier coefficients, $A_{k,m}$ and $B_{k,m}$.
3. Convert $A_{k,m}$ and $B_{k,m}$ into the spherical harmonic coefficients, $\mathrm{ar}_{n,m}$ and $\mathrm{ai}_{n,m}$.
4. Divide $\mathrm{ar}_{n,m}$ and $\mathrm{ai}_{n,m}$ by $-n(n+1)$. This step corresponds to the inverse Laplacian operation in spherical harmonic space.

5. Convert the resulting spherical harmonic coefficients back into the spherical Fourier coefficients, $\tilde{A}_{k,m}$ and $\tilde{B}_{k,m}$.
6. Transform $\tilde{A}_{k,m}$ and $\tilde{B}_{k,m}$ back into physical space using the inverse spherical Fourier transform to obtain the triangularly truncated stream function and velocity potential.
7. Reconstruct the truncated wind velocity vector by calculating the spatial derivatives of the stream function and velocity potential.

The inverse Laplacian operation described above cannot be replaced by solving the Poisson equation directly using the spherical Fourier transform method proposed by Yee [23]. Our numerical experiments confirm that the approach using Yee's Poisson solver induces numerical instability within only a few time steps of integration.

4 Evaluation Using Shallow-Water Test Cases

We conducted Test Cases 1 and 2 proposed by Williamson [21]. Test Case 1 is a linear advection problem, whereas Test Case 2 is a nonlinear steady-state problem. The three methods compared are as follows:

(i) **New spherical Fourier transform method.**
A pseudo-spectral method combining the one-dimensional Fourier transform described in Sect. 2 with the isotropic wavenumber truncation described in Sect. 3.

(ii) **Combined method.**
A pseudo-spectral method combining the one-dimensional Fourier transform described in Sect. 2 with the isotropic wavenumber truncation based on the spherical harmonic transform.

(iii) **Spherical harmonic transform method.**
A Galerkin spectral method based on the spherical harmonic transform.

The third method is one of the standard approaches widely utilized in atmospheric dynamics.

4.1 Governing Equations

The shallow water equations on a sphere can be expressed as follows:

$$\begin{aligned}
\frac{\partial u}{\partial t} &= -u\delta - \frac{v}{a}\frac{\partial u}{\partial \theta} + \frac{u}{a}\frac{\partial v}{\partial \theta} + fv - \frac{1}{a\cos\theta}\frac{\partial \phi}{\partial \lambda} \\
\frac{\partial v}{\partial t} &= -u\zeta - \frac{u}{a}\frac{\partial u}{\partial \theta} - \frac{v}{a}\frac{\partial v}{\partial \theta} - fu - \frac{1}{a}\frac{\partial \phi}{\partial \theta} \\
\frac{\partial \phi}{\partial t} &= -\phi\delta - \frac{u}{a\cos\theta}\frac{\partial \phi}{\partial \lambda} - \frac{v}{a}\frac{\partial \phi}{\partial \theta}
\end{aligned} \tag{14}$$

where t is time, u and v are the zonal and meridional wind components, and ϕ is the geopotential height. The terms ζ and δ denote vorticity and divergence,

respectively. The constants g, a, and f represent the acceleration due to gravity, the radius of the Earth, and the Coriolis parameter. In particular, the geopotential height is defined as:

$$\phi = gh^\star = g(h - h_s) \tag{15}$$

where $h^\star$ is the depth of the fluid and h is the height of the free surface above a reference sphere. All methods employed a regular latitude-longitude grid. The numerical libraries utilized were FFTW (v3.3.10; [8]) and SPHEREPACK 3.2 [1]. We used SPHEREPACK 3.2 because it includes the spherical harmonic expansion method on a regular latitude-longitude grid proposed by Swarztrauber [18].

4.2 Williamson Test Case 1

Test Case 1 is to simulate cosine bell advection. The cosine bell was initially positioned on the equator at $\lambda = \pi/2$. The radius and height of the bell were set to $1/3$ rad and 1000 m, respectively. The bell is advected around the sphere, completing one revolution in 12 days while crossing both poles. Only the geopotential height is evolved over time, without evolving the horizontal wind components. The initial state is shown in Fig. 1.

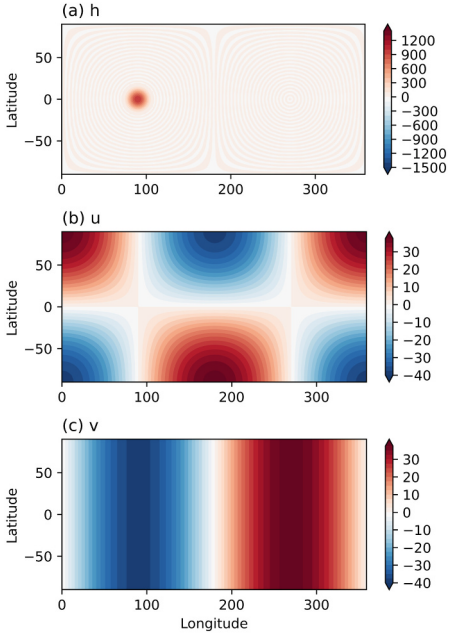

Fig. 1. Initial states for Test Case 1 using the proposed method with a truncation wavenumber of 85. (a) geopotential height, (b) zonal and (c) meridional wind components.

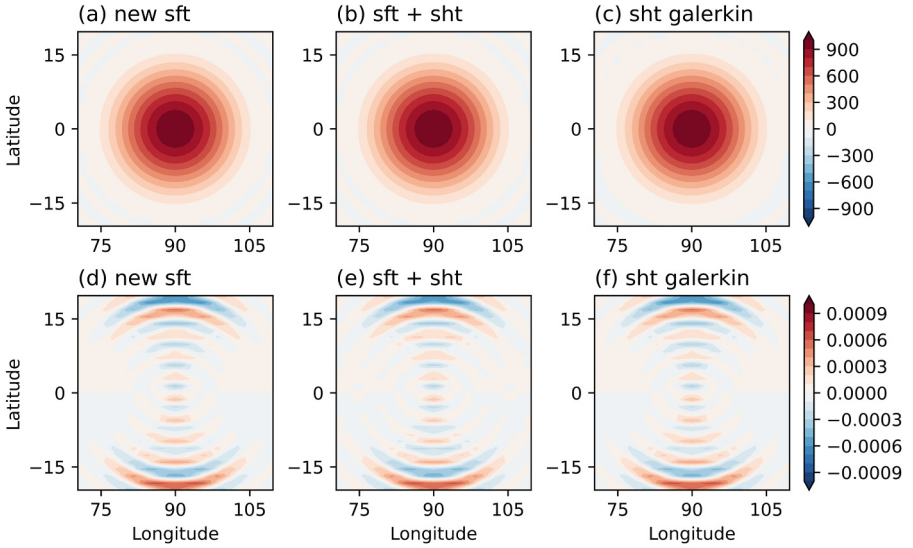

Fig. 2. Simulated states after 12 days for Test Case 1. The truncation wavenumber is 85. (a,d) the proposed method, (b,e) the combined method and (c,f) the spherical harmonic method, and (a–c) and (d–f) show the geopotential height and the error distribution of the geopotential height, respectively.

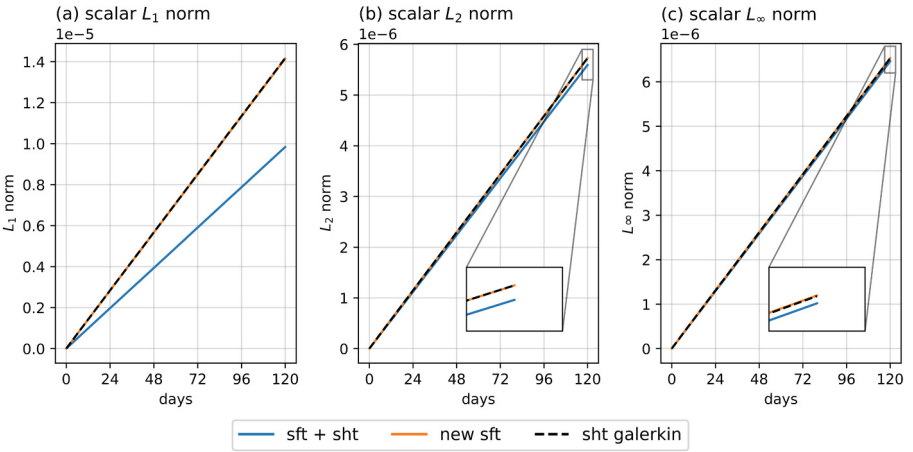

Fig. 3. Error norms for Test Case 1 over a 120 day integration. The truncation wavenumber is 85.

While error patterns show little difference among the methods after 12 days (Fig. 2), the proposed method demonstrates superior accuracy in the error norms over a 120-day integration (Fig. 3). These scalar error norms are evaluated fol-

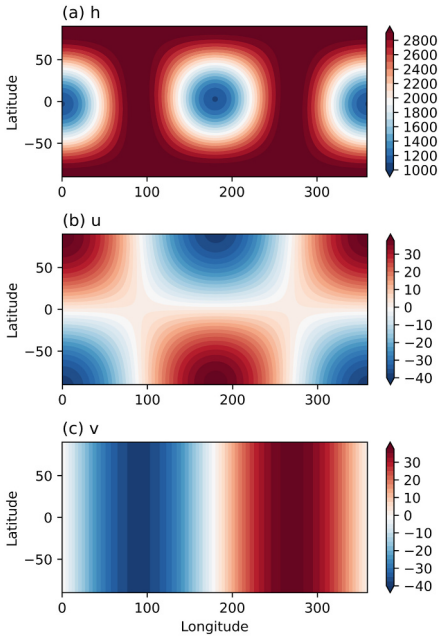

Fig. 4. Same as Fig. 1 but for Test Case 2.

lowing Eqs. (82)–(84) of [21]. Note that the initial conditions for all methods were pre-truncated in wavenumber space.

4.3 Williamson Test Case 2

Test Case 2 is a nonlinear advection experiment that maintains an initial state in geostrophic balance. In this experiment, the angle between the flow's axis of rotation and the Earth's rotation axis was set to $\pi/2 - 0.05$ to intentionally introduce a discontinuity in the wind vector at the poles (Fig. 4).

Regarding the horizontal error distribution of the geopotential height, the proposed method and the combined method show very similar patterns (Fig. 5a,c). In contrast, the spherical harmonic method exhibits prominent noise parallel to the latitude lines (Fig. 5e). For the error distribution of the horizontal wind component, on the other hand, the combined method and the spherical harmonic method show similar characteristics, whereas the proposed method exhibits an error pattern characterized by the zonal wavenumber 1 mode (Fig. 5b,d,f, v is similar to u in behavior).One possible cause of this error pattern is that the vector wavenumber truncation procedure (Sect. 3.2) requires multiple intermediate transformations between the vorticity-divergence fields and the velocity components. These additional steps, compared to the simpler scalar truncation, make the vector field more susceptible to the accumulation of numerical rounding errors.

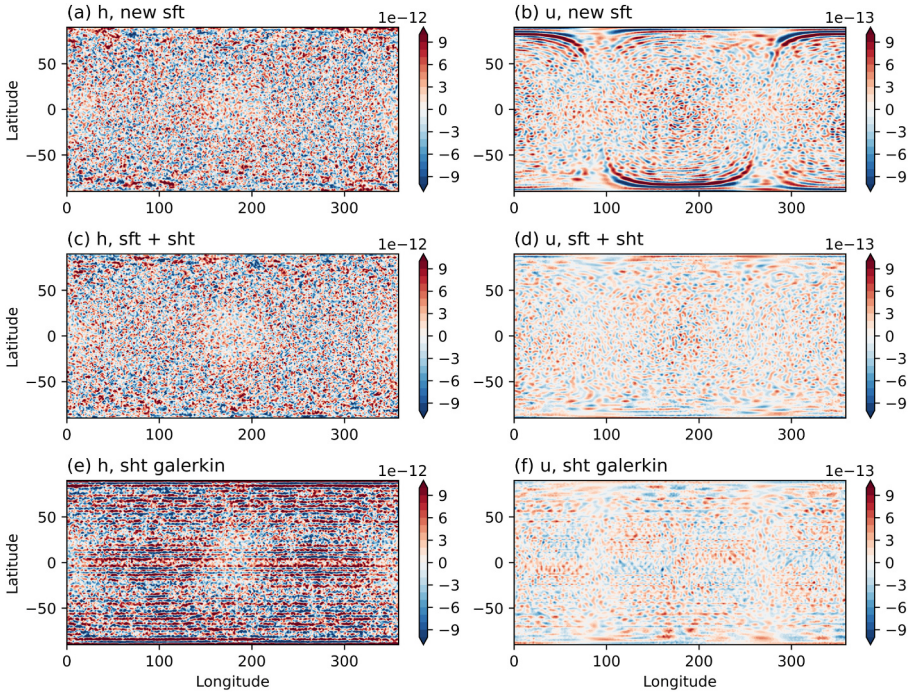

Fig. 5. Error distribution after 10 days for Test Case 2. The truncation wavenumber is 85. (a,b) the proposed method, (c,d) the combined method, and (e,f) the spherical harmonic method. Panels (a,c,e) and (b,d,f) show the error distribution of the geopotential height and zonal wind, respectively.

Nevertheless, evaluating both scalar and vector error norms using Eqs. (97)–(99) of [21] reveals that the proposed method maintains high accuracy in scalar fields even if the vector precision is lower than that of other methods. This demonstrates that the overall utility of the proposed method remains robust (Fig. 6).

5 Preliminary Benchmark of Computation Time

The proposed method consists of the spatial differentiation method described in Sect. 2 and the wavenumber truncation method described in Sect. 3. The spatial differentiation can be computed independently along latitudes and longitudes. Similarly, the wavenumber truncation can derive spherical Fourier coefficients independently in the latitudinal and longitudinal directions. Furthermore, the mutual transformation with spherical harmonic coefficients can be calculated independently for each zonal and meridional wavenumber, resulting in highly efficient parallelization. To demonstrate this advantage, we compared our method with SHTns [15], which implements the world's fastest spherical harmonic transform algorithm [13].

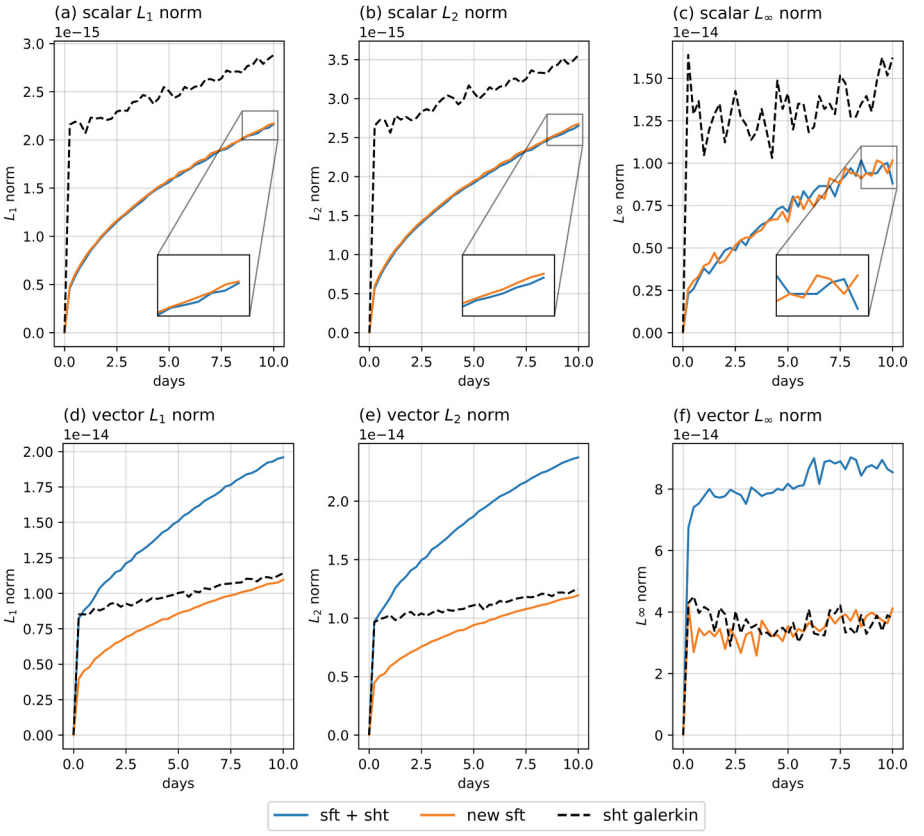

Fig. 6. Same as Fig. 3 but for Test Case 2. (a–c) scalar error norm, (d–g) vector error norm.

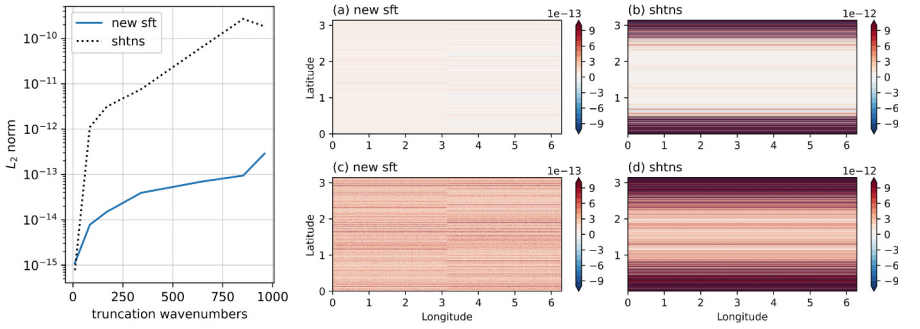

Fig. 7. Error of the proposed method and SHTns. Left panel shows the L_2 error norms. Right panel shows the error distribution in the physical space, (a,c) the proposed method and (b,d) SHTns. The truncation wavenumbers are (a,b) 639, (c,d) 959.

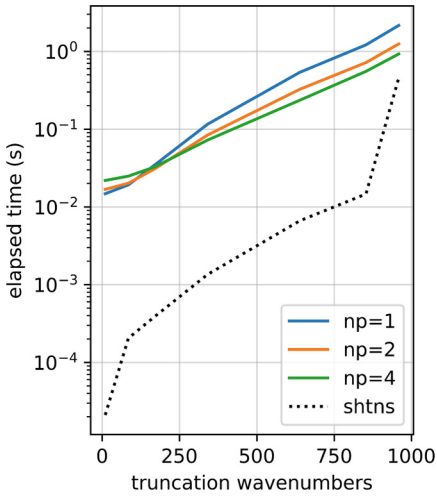

Fig. 8. Execution time for the proposed method and SHTns. Abscissa represents the numbers of truncation wavenumbers, and ordinates represents the execution time. np is parallelization number in Coarray Fortran. shtns parallelized with OpenMP using 64 threads.

The proposed method was parallelized using Fortran Coarrays, which were introduced in the Fortran 2008 standard. In contrast, the SHTns was compiled with OpenMP support and executed on 64 threads. The computational environment consisted of FreeBSD 14.3-RELEASE-p3 equipped with an AMD Ryzen Threadripper PRO 3975WX CPU (32 cores, 64 threads) and 256 GB of RAM.

For the benchmark test, we evaluated the computation of a gradient from a scalar field followed by wavenumber truncation. The input scalar was defined as follows:

$$f(\theta, \lambda) = \cos(2\theta) \tag{16}$$

The spherical Fourier transform method employed a regular latitude-longitude grid that includes the poles, whereas the spherical harmonic transform method utilized a Gaussian grid. Additionally, because SHTns performs the spherical harmonic transform at a predefined resolution, explicit wavenumber truncation is unnecessary.

First, we compare only the latitudinal component of the gradient. The error in the method using the spherical Fourier transform is approximately $O(10^{-2})$ smaller than that of the method using SHTns, indicating higher accuracy. In particular, a significant difference is observed in the error distribution near the poles (Fig. 7). SHTns employs a three-term recurrence relation to compute the associated Legendre functions [13,15]. At high resolutions, this method is prone to numerical underflow near the poles. Furthermore, it has been pointed out that computing the associated Legendre functions using a three-term recurrence relation yields lower accuracy compared to using a four-term recurrence relation

[6,7]. In contrast, the spherical Fourier transform maintains numerical stability and high accuracy even at high resolutions.

Next, we evaluate the computational performance by comparing the execution times of the two methods. To minimize the impact of background system processes, the computation was repeated 100 times, and the minimum execution time recorded across all trials is presented in Fig. 8.

The Coarray method was not faster than the SHTns method at resolutions with truncation wavenumbers of 1000 or less. However, as the excution time for the SHTns method increases sharply when the truncation wavenumber exceeds approximately 800, the spherical Fourier transform method may offer faster computation for high-resolution calculations. In the present study, the verification was limited to resolutions up to truncation wavenumbers of 1000 due to available computational resources and current implementation constraints. Performance evaluation at higher resolutions remain as a subject for future work.

6 Conclusions

We have developed a spherical Fourier transform method that achieves faster computation compared to the spherical harmonic transform. While numerical challenges remain in calculating vector quantities due to the complexity of the intermediate transformations, the proposed method achieves higher accuracy for scalar fields. This method possesses two novel features absent in previously proposed spherical Fourier transform approaches:

- The problem of the pole singularity is resolved by applying a specific formulation at the poler points, distinct from that used for non-poler grids. This enables the method to accommodate regular latitude-longitude grids that include the poles.
- By employing an isotropic wavenumber truncation on the sphere constructed solely with Fourier transforms, the method enables numerically stable and highly accurate computations.

These features facilitate the efficient solution of time-dependent partial differential equations on the sphere. Furthermore, because both of these features can be formulated without modifying the basis of the Fourier transform, there is no need to solve a system of linear equations to transform the coefficients. Consequently, the method can be implemented simply by utilizing any standard library capable of performing forward and inverse one-dimensional Fourier transforms.

Acknowledgments. The authors thank three anonymous reviewers for their constructive comments. This work was supported by JSPS KAKENHI Grant Number 24H00021 and JST K Program Grant Number JPMJKP25Q1, and was conducted as part of the collaborative research program (2026NE-01) of the Disaster Prevention Research Institute, Kyoto University.

References

1. Adams, J.C., Swarztrauber, P.N.: SPHEREPACK 3.0: a model development facility. Mon. Wea. Rev. **127**(8), 1872–1878 (1999). https://doi.org/10.1175/1520-0493(1999)127<1872:SAMDF>2.0.CO;2
2. Boyd, J.P.: The choice of spectral functions on a sphere for boundary and eigenvalue problems: a comparison of chebyshev, fourier and associated legendre expansions. Mon. Wea. Rev. **106**(8), 1184–1191 (1978). https://doi.org/10.1175/1520-0493(1978)106<1184:TCOSFO>2.0.CO;2
3. Cheong, H.B.: Application of double Fourier series to the shallow-water equations on a sphere. J. Comput. Phys. **165**(1), 261–287 (2000). https://doi.org/10.1006/jcph.2000.6615
4. Cheong, H.B.: Double Fourier series on a sphere: applications to elliptic and vorticity equations. J. Comput. Phys. **157**(1), 327–349 (2000). https://doi.org/10.1006/jcph.1999.6385
5. Cooley, J.W., Tukey, J.W.: An algorithm for the machine calculation of complex Fourier series. Math. Comp. **19**(90), 297–301 (1965). https://doi.org/10.2307/2003354
6. Enomoto, T.: Comparison of computational methods of associated Legendre functions. SOLA **11**, 144–149 (2015). https://doi.org/10.2151/sola.2015-033
7. Enomoto, T., Kuwano-Yoshida, A., Komori, N., Ohfuchi, W.: Description of AFES 2: improvements for high-resolution and coupled simulations. In: High Resolution Numerical Modelling of the Atmosphere and Ocean, pp. 77–97. Springer, New York, NY (2008). https://doi.org/10.1007/978-0-387-49791-4_5
8. Frigo, M., Johnson, S.: The design and implementation of FFTW3. Proc.IEEE **93**(2), 216–231 (2005). https://doi.org/10.1109/JPROC.2004.840301
9. Fukushima, T.: Fast computation of sine/cosine series coefficients of associated Legendre function of arbitrary high degree and order. J. Geod. Sci. **8**(1), 162–173 (2018). https://doi.org/10.1515/jogs-2018-0017
10. Fukushima, T.: Transformation between surface spherical harmonic expansion of arbitrary high degree and order and double Fourier series on sphere. J. Geod. **92**(2), 123–130 (2018). https://doi.org/10.1007/s00190-017-1049-3
11. Gruber, C., Abrykosov, O.: On computation and use of Fourier coefficients for associated legendre functions. J. Geodesy **90**(6), 525–535 (2016). https://doi.org/10.1007/s00190-016-0891-z
12. Hofsommer, D.J., Potters, M.L.: Table of fourier coefficients of associated legendre functions : repr. from Proceedings of the KNAW, ser. A. Proceedings of the Koninklijke Nederlandse Akademie van Wetenschappen: Series A: Mathematical Sciences **63**(5), 460–480 (1960). https://ir.cwi.nl/pub/8862
13. Ishioka, K.: A new recurrence formula for efficient computation of spherical harmonic transform. J. Meteor. Soc. Japan **96**(2), 241–249 (2018). https://doi.org/10.2151/jmsj.2018-019
14. Orszag, S.A.: Fourier series on spheres. Mon. Wea. Rev. **102**(1), 56–75 (1974). https://doi.org/10.1175/1520-0493(1974)102<0056:FSOS>2.0.CO;2
15. Schaeffer, N.: Efficient spherical harmonic transforms aimed at pseudospectral numerical simulations. Geochem. Geophys. Geosyst. **14**(3), 751–758 (2013). https://doi.org/10.1002/ggge.20071
16. Schuster, A.: On some definite integrals, and a new method of reducing a function of spherical co-ordinates to a series of spherical harmonics. Philos. Trans. A Math Phys. Eng. Sci. **200**(321–330), 181–223 (1903). https://doi.org/10.1098/rsta.1903.0004

17. Spotz, W.F., Taylor, M.A., Swarztrauber, P.N.: Fast shallow-water equation solvers in latitude-longitude coordinates. J. Comput. Phys. **145**(1), 432–444 (1998). https://doi.org/10.1006/jcph.1998.6026
18. Swarztrauber, P.N.: On the spectral approximation of discrete scalar and vector functions on the sphere. SIAM J. Numer. Anal. **16**(6), 934–949 (1979). https://doi.org/10.1137/0716069
19. Swarztrauber, P.N.: Vectorizing the FFTs. In: Parallel Computations, pp. 51–83. Academic Press (1982). https://doi.org/10.1016/B978-0-12-592101-5.50007-5
20. Swarztrauber, P.N.: The vector harmonic transform method for solving partial differential equations in spherical geometry **121**, 3415–3437 (1993). https://doi.org/10.1175/1520-0493(1993)121<3415:TVHTMF>2.0.CO;2
21. Williamson, D.L., Drake, J.B., Hack, J.J., Jakob, R., Swarztrauber, P.N.: A standard test set for numerical approximations to the shallow water equations in spherical geometry. J. Comput. Phys. **102**(1), 211–224 (1992). https://doi.org/10.1016/S0021-9991(05)80016-6
22. Yee, S.Y.K.: Studies on Fourier series on spheres. Mon. Wea. Rev. **108**(5), 676–678 (1980). https://doi.org/10.1175/1520-0493(1980)108<0676:SOFSOS>2.0.CO;2
23. Yee, S.Y.K.: Solution of Poisson's equation on a sphere by truncated double Fourier series. Mon. Wea. Rev. **109**(3), 501–505 (1981). https://doi.org/10.1175/1520-0493(1981)109<0501:SOPEOA>2.0.CO;2
24. Yoshimura, H.: Improved double Fourier series on a sphere and its application to a semi-implicit semi-Lagrangian shallow-water model. Geosci. Model Dev. **15**(6), 2561–2597 (2022). https://doi.org/10.5194/gmd-15-2561-2022